Research Square

Preprints are preliminary reports that have not undergone peer review.
They should not be considered conclusive, used to inform clinical practice,
or referenced by the media as validated information.

Enhanced mercury accumulation links to terrestrial carbon mobilization during the PETM

Gong Yanjie

gyj2008vip@163.com

PetroChina Research Institute of Petroleum Exploration and Development

Theodore R. Them

College of Charleston

Caineng Zou

PetroChina Research Institute of Petroleum Exploration and Development https://orcid.org/0000-0001-5912-1729

Joost Frieling

Thomas Algeo

University of Cincinnati

Clara Meier

Ruoyu Sun

Tianjin University https://orcid.org/0000-0001-7261-8377

Article

Keywords: carbon release, carbon oxidation, Mid-Atlantic Shelf, New Jersey

Posted Date: August 11th, 2026

DOI: https://doi.org/10.21203/rs.3.rs-10266619/v1

License: This work is licensed under a Creative Commons Attribution 4.0 International License.
Read Full License

Additional Declarations: There is **NO** Competing Interest.

Abstract

The Paleocene–Eocene Thermal Maximum (PETM) coincided with North Atlantic Igneous Province emplacement, but volcanic versus surface carbon sources remain debated. Here, we present high resolution Hg concentration and isotope data from the United States Mid-Atlantic Shelf, revealing a pronounced Hg increase (2–3 times background) coincident with the PETM onset, together with a significant negative shift in Δ^{199}Hg (down to − 0.24‰). A Hg isotope mixing model indicates that more than half of the Hg was derived from terrestrial soil or sedimentary rocks. Mercury is often stored in vegetation, soils and sedimentary rocks in close association with organic matter, and the Hg-isotope evidence for enhanced Hg release from these reservoirs provides further evidence for enhanced organic carbon oxidation. We explore whether these Hg data can be used as an independent approach to quantitatively assess total organic carbon (including both fossil and soil carbon) oxidation due to terrestrial erosion. Our estimates arrive at ~ 1400 Pg C release under an average scenario and up to ~ 4520 Pg C (upper limit), supporting the hypothesis that terrestrial carbon mobilization constituted an important contributor to a positive feedback on PETM hyperwarming.

Introduction

The Paleocene-Eocene Thermal Maximum (PETM, ca. 55.9 million years ago [Ma]) has the potential to provide valuable insights into the impact of deep-time carbon-cycle perturbations on climate and ecosystem evolution. Carbon isotope records from the PETM display a rapid and sustained negative carbon isotope excursion (CIE)[1] that appears to follow an initial warming phase[2]. Overall, the PETM is marked by a global surface ocean warming of 5°C[3] and major environmental changes that affected marine and terrestrial ecosystems, including enhanced hydrological cycling[4, 5], and erosion[6]. Several scenarios regarding the origin of the CIE and climate warming have been proposed, including the emplacement of the North Atlantic Igneous Province (NAIP)[7]. The PETM however occurs during a multi-million year warming trend, during which many similar events occur[8] that do not align with the main emplacement phase of the NAIP. The orbital pacing of the pre- and post-PETM hyperthermals, likely driven predominantly by surface carbon cycle feedback processes, raises questions how NAIP volcanism and surface feedbacks may have shaped the PETM.

It is often proposed that NAIP emplacement could have forced late Paleocene and part of the PETM warming[9] through CO_2 emissions from flood basalt eruptions and part of the CIE may be the result of isotopically depleted thermogenic carbon emissions around the time of the PETM[10]. Regardless of the original trigger, there is evidence that climate warming activated several surface carbon cycle feedbacks. The climate-sensitive positive feedback systems includes mostly isotopically depleted organic-derived carbon reservoirs, such as carbon dioxide and methane produced by the decomposition of organic matter in thawing high-latitude permafrost or peat[11], vegetation loss[12], kerogen weathering[13, 14]. Similar to volcanic activity, each of these terrestrial organic carbon reservoirs might perturb the global Hg cycle

due to the close association of Hg and organic-matter and they may enrich marine sediments after mobilization of terrestrial Hg, leaving an isotopically distinct signature[15].

Although mercury concentration anomalies have been reported from some PETM sites[16], no notable anomaly is apparent at other sites, primarily those in deep-sea settings, including 25/11–7[17], 23/16b-9[18] and 30/14–1[16] from the North Sea, Zumaia[19] from the Pyrenean foreland basin, and IODP Site 1262[16] from the South Atlantic. Moreover, the timing of sedimentary Hg enrichments during the PETM was not synchronous globally. The global CIE allows sedimentary records from different sites to be divided into pre-CIE, CIE and post-CIE stages, enabling robust inter-site comparisons[20]. For instance, Hg anomalies are observed at the onset of the CIE in the North Sea Basin (22/10a-4 and E-8X[9]), at both the onset and end of the CIE at Fur Island[17], but in the mid CIE of the Lussagnet, Serraduy, and Esplugafreda sections from the Pyrenean foreland basin[19]. Mercury isotope data, an effective method for assessing Hg depositional pathways in sediments, have been published to date only for the 23/16b-9 site in the North Sea[18]. These differences among PETM sites may point to local controls on Hg cycling rather than direct emissions from the NAIP.

Here, we investigate Hg geochemical data from the Mid-Atlantic Shelf east of New Jersey and Maryland in the United States (U.S.), which represent some of the most expanded and stratigraphically continuous records of the PETM[21, 22]. Evidence for deep soil erosion[23] and fossil carbon mobilization[12, 14] in the hinterland makes this area ideally suited for clarifying the sources and timing of Hg and carbon emissions during the PETM. We studied three drill cores[21, 22] from the inner to outer shelf [24] (Fig. 1A, B): the Wilson Lake (WL; 39°39'20.9"N, 75°2'31.2"W; 100–150 m water depth[24]) in New Jersey, and the Cambridge Dorchester Airport (CD; 38°52'58.8"N, 76°3'0"W; 30–100 m water depth[25]) and South Dover Bridge (SDB; 38°44'49.0"N, 76°0'25.0"W ; ~100 m water depth[26]) in Maryland. These sites experienced subtropical climates during the PETM[27], subject to enhanced seasonal precipitation[28, 29], and the more proximal sites were at times influenced by terrestrial/fluvial input[29]. The P/E boundary sequence consists of two sedimentary units confined to the Salisbury Embayment: the Aquia Formation (upper Paleocene), Marlboro Clay (lower Eocene)[21]. The study interval encompasses the transition from glauconite-rich quartz sands of the Aquia Formation to silty clays and clays of the Marlboro Clay[21]. High sedimentation rates during the early PETM, in some locations up to 50 cm/kyr[30], provide high temporal resolution through the event interval. In this study, we analyzed 22 samples for Hg isotopes and 159 samples for Hg concentrations through the CIE, enabling a robust assessment of Hg delivery and sources.

Samples and Methods

All samples analyzed were collected from drill cores. Prior to pulverization, each sample was inspected to ensure freshness and rinsed with deionized water to minimize potential contamination from drill mud. Guided by existing carbon isotope data[14, 22], samples (n = 159) were taken at ~ 0.2 m (CIE) or ~ 0.5 m

intervals to ensure sufficient coverage of Hg behavior from the late Paleocene to the PETM CIE. Based on Hg concentration results, 22 representative samples covering the PETM as well as pre- and post-PETM intervals were subsequently chosen for Hg isotopic analysis. The analysis of Hg concentrations and isotopes was conducted at the College of Charleston and Tianjin University, respectively. See detailed description of methods in the Supplemental Note 1.

Results

In the background intervals above and below the CIE at the three sites, Hg concentrations are generally low (< ~ 10 ng/g), whereas within the CIE, Hg concentrations increase to an average of 25–35 ng/g (maximum 42 ng/g) (Fig. 2A – C). Total organic carbon (TOC) is low, generally < 1%, with only one sample from CD exceeding 1% (Fig. 2C). However, TOC within the PETM shows an increase of up to 2–3× above background levels (Fig. 2A – C). Detailed elemental data from WL[16] allowed analysis of Hg concentrations with various host phases such as TOC, total sulfur (TS), aluminum (Al), manganese (Mn), and iron (Fe). In terms of average values, Hg/TOC increased from 31.6 ng/g/wt% in the pre-CIE background interval to 76.2 ng/g/wt% within the CIE, Hg/TS increased from 155.0 ng/g/wt% to 302.9 ng/g/wt%, Hg/Al from 4.5 ng/g/wt% to 8.9 ng/g/wt%, Hg/Mn from 0.1 to 0.2 (ng/g)/(mg/kg), and Hg/Fe from 2.0 ng/g/wt% to 6.0 ng/g/wt%. These ratios are generally 2–3× higher within the CIE relative to background levels, demonstrating the increase in Hg drives the change in normalized Hg. To eliminate masking or amplification effects from excessive or insufficient TOC on mercury signals, we calculated excess mercury content using robust non-linear fitting[31], considering it alongside Hg and Hg/TOC to identify anomalous mercury signals. The data show that maximum Hg_{xs} values increased from 7.24ng/g (pre-PETM) to 20.9 ng/g (PETM) in WL, 1.92 ng/g to 18.4 ng/g in CD (Fig. 3B). The Δ^{199}Hg MIF background signal (pre- and post-CIE) shows significantly positive values (average + 0.07‰, maximum + 0.16‰), whereas within the CIE, it shows distinctly negative values (average – 0.03‰, minimum – 0.08‰, Fig. 2A – C), with an average negative excursion amplitude of – 0.1‰ and a maximum of – 0.24‰. Detailed description of the Hg isotope data is provided in the Supplemental Notes 2 – 3.

Discussion

Hg Anomalies and Negative Hg Isotope Excursions

Our data reveal elevated Hg concentrations during the PETM, indicating an average excess Hg load 2–3× above background levels (Fig. 2A – C), on top of a simultaneous increase in the delivery of siliciclastic material. This provides evidence of relative Hg enrichment in the stratigraphic sequence.

The odd-isotope fractionation of Hg (Δ^{199}Hg, MIF) is primarily generated by photochemical reduction during atmospheric transport. Therefore, combining Δ^{199}Hg with Hg concentration enrichments can help identify the source(s) and/or transport pathways of excess Hg[32, 33]. Direct volcanic emissions from the mantle are typically considered to have Δ^{199}Hg close to 0‰. Gaseous Hg emitted by volcanoes

undergoes long-range atmospheric transport where Hg(0) is converted to Hg(II). This Hg(II) acquires positive Δ^{199}Hg, whereas terrestrial plants and soils that absorb Hg(0) exhibit negative Δ^{199}Hg[15]. Apart from anthropogenic emissions, the primary sources of Hg in soils today are the uptake of atmospheric Hg(0) by vegetation (followed by litterfall) and direct absorption of Hg(0) by soils, rather than the deposition of atmospheric Hg(II)[32].

Sediments from the three U.S. Mid-Atlantic Shelf study sites have pre-PETM background Δ^{199}Hg averaging + 0.1‰, with a maximum of + 0.16‰ (Fig. 3A). These values also gradually return to positive MIF after the PETM, which is consistent with offshore marine sediments typically having relatively positive Hg isotope values[32]. Before and after the PETM, the primary Hg depositional flux to the study sites likely originated from atmospheric wet deposition (primarily as Hg(II)). A major contribution of Hg derived from soil erosion and terrestrial plant debris (negative Δ^{199}Hg), or rock erosion with negative Δ^{199}Hg is incompatible with the pre-PETM positive background MIF (Fig. 3B). During the PETM, the Δ^{199}Hg data from the three study sites exhibit consistent and pronounced negative anomalies, with a maximum negative excursion of − 0.24‰ (Fig. 3A). In most PETM samples analyzed here Δ^{199}Hg ranges from ca. −0.1‰ to 0‰, which align most closely with the Hg isotopic signature of mixing in from soils (predominantly distributed in the range of − 0.2‰ to 0‰[34]) (Fig. 3B). In contrast, terrestrial plants typically show Δ^{199}Hg between − 0.4‰ and − 0.2‰[34], while exclusively volcanic Hg transported through the atmosphere and deposited in marine environments is primarily distributed in the range of 0‰ to + 0.2‰[34] (Fig. 3B). Such negative excursions in Hg-MIF in combination with overall higher concentrations therefore reflect an increased Hg load from negative Δ^{199}Hg sources. Though Hg volatilized around igneous sills and dykes may carry negative Δ^{199}Hg depending on the host rock, the NAIP thermogenic volatiles were dominantly released in submarine settings, which, combined with the low temperatures at the top of the vents, limits the reach of thermogenic Hg emissions to the direct vicinity of the source. Other local effects that produce negative MIF such as diagenetic overprinting in sulfidic pore waters, photic zone euxinia or even extra-terrestrial input can also be excluded as there is no evidence for these in the same intervals as where negative Hg-MIF excursions are observed (Supplemental Note 2). We hence consider a terrestrial plant, soil or rock-derived origin of the negative MIF signal the most parsimonious explanation.

Terrestrial Hg input may derive from vegetation, soils and bedrock. The most direct release of Hg may occur from vegetation during wildfires. Studies focused on vegetation and wildfire activity from the PETM have been conducted at both WL and Bass River (BR) sites in the present study area[35, 36]. On average, there is no clear increase in the flux of graphitic black carbon (GBC), a byproduct of combustion, during the PETM[36]. Moreover, a recent study suggested that vegetation cover in the hinterland was strongly reduced during the body of the PETM CIE, the interval where the most negative Hg-MIF is observed[37]. These data argue against a vegetation-derived Hg influence on the MIF signal. However, reduced vegetation cover increases the likelihood of enhanced soil mobilization, sedimentary rock and bedrock erosion, which may include Appalachian Pennsylvanian-age coal deposits, all of which can also

release appreciable amounts of Hg with a negative MIF signature. However, the coals are a proportionally small volume of all the rocks in a river catchment that can be eroded[37] and their Hg content is generally not high[38] either.

Intensified erosion during PETM

An accelerated hydrological cycle and enhanced soil erosion during the PETM have been robustly demonstrated[4, 5]. While precipitation shifts primarily manifest as seasonal variations and heightened climate extremes rather than global-scale humidification[1], mid-to-high latitudes in the Northern Hemisphere experienced markedly increased rainfall[28], perhaps at times further amplified by orbital eccentricity. Proxy records and modeling show that due to warmer climate and specific orbital configurations, precipitation in coastal New Jersey may have increased by as much as 2–3 fold during the PETM relative to the late Paleocene[28]. The erosion would increase because of vegetation loss and more open landscapes even without seasonal precipitation extremes[12]. Concurrently, increased siliciclastic sediment flux, higher sediment accumulation rates, delivery of pre-aged carbon and changes in clay mineralogy in marginal seas all point to deeper physical erosion at U.S. east coast during the PETM[14, 23].

An intensified hydrological cycle and erosion on land increased the Hg flux into the coastal oceans. Negative lithium isotope excursions and the influx of large amounts of clay indicate that global erosion rates may have increased by a factor 2–3 over > 100 kyr, significantly enhancing terrestrial inputs to the oceans[6]. It is important to note that riverine transport introduces not only terrestrial soil and ancient sedimentary rock sources (Δ^{199}Hg range of − 0.2‰ to 0‰ and − 0.4‰ to − 0.2‰, respectively) but also Hg from bedrock weathering (Δ^{199}Hg ≈ 0‰, similar to mantle sources[39, 40]). Therefore, the MIF value of Hg delivered by rivers should be less negative than that of pure terrestrial soil Hg and ancient sedimentary rock sources, which is consistent with Δ^{199}Hg values from the study sites (ca. −0.1‰).

In marine settings, atmospheric Hg(0) deposition primarily occurs through air-sea exchange where the ocean absorbs Hg(0)[41], while atmospheric Hg(II) deposition mainly enters the ocean via precipitation[32]. The positive Hg isotope background values before and after the PETM indicate that the sedimentary Hg source was dominated by atmospheric Hg(II). During the PETM, under conditions of an enhanced hydrological cycle, this phenomenon should have been even more pronounced because at face value increased precipitation would further enhance Hg(II) wet deposition over dry deposition[32]. Therefore, the Hg MIF signal during the PETM would likely have become more positive due to increased Hg(II) wet deposition if there was no Hg source change such as increased terrestrial Hg delivery. The overall signature is hence interpreted as a mixed signal combining riverine-transported Hg (MIF from combined terrestrial sources between − 0.2‰ and ~ 0‰) and wet-deposited Hg(II) (MIF between ~ 0‰ and + 0.2‰) (Fig. 3B), whereby the terrestrial Hg sources outcompeted the Hg(II) wet deposition flux, resulting in negative MIF excursions.

The mass-dependent Hg isotope fractionation data also support the hypothesis that terrestrial Hg inputs increased via riverine fluxes. For δ^{202}Hg, atmospheric deposition typically exhibits a wide range (~ − 2‰ to ~ + 2‰) of δ^{202}Hg values, whereas terrestrial Hg input from rivers, which inherits its signature from soils and vegetation, generally yields more negative δ^{202}Hg[32, 33]. The average δ^{202}Hg from the three sites is − 1.02‰ before the PETM and − 1.11‰ during the PETM (Fig. 2A − C) and the difference is not statistically significant (p = 0.49, two-tailed t-test). This argues against a dominantly atmospheric source for the mercury and is instead consistent with terrestrial Hg delivered by rivers. Mass-independent fractionation of even isotopes (Δ^{200}Hg) occurs in the upper atmosphere and is unaffected by Earth's surface biogeochemical processes, making it an effective tracer for distinguishing between dry and wet atmospheric deposition pathways and processes[32, 33]. However, also because of these characteristics, the range of Δ^{200}Hg variation is smaller compared to Δ^{199}Hg. Consequently, its changes during geological events are often less pronounced and analytically more difficult to resolve than those of Δ^{199}Hg (Figs. 2A − C and 4B). If the Hg was derived from atmospheric deposition following release by wildfires or contact metamorphism of organic-rich sediments, Δ^{200}Hg and Δ^{199}Hg would inherit the original negative MIF signals and, after atmospheric transport and photoreduction reactions, would typically show a strong correlation and negative values[42]. In contrast, if the source was soil erosion leading to riverine input, this correlation is generally weaker, and Δ^{200}Hg values are not exclusively negative because the negative even-MIF signal mixes with Hg from wet deposition (positive Δ^{200}Hg)[32]. The Δ^{200}Hg data range from the three sites (− 0.1‰ to + 0.1‰) aligns more closely with the soil erosion (Fig. 4B). Furthermore, the Δ^{199}Hg and Δ^{200}Hg data from the WL and SDB sites show no correlation (R^2 = 0.013; n = 15; p = 0.69, Fig. 4C). Indeed, fluvial input can effectively preserve the terrestrial Hg signal, as Hg in rivers is typically transported bound to soil particles, clay minerals, or organic matter[43]. In contrast, Hg transported atmospherically as Hg(0) can be considered to be more susceptible to alteration through photochemical reactions[33]. This explains why the Δ^{199}Hg signal range from the three sites (~ − 0.1‰) corresponds relatively well with a (modern) soil signal (− 0.2‰ to 0‰), indicating that rivers represent the more likely source of Hg for the study sites. A global Hg isotope comparison during the PETM is provided in Supplemental Note 3.

Can Hg mobilization further constrain oxidation of terrestrial carbon during the PETM?

During the PETM, sediment accumulation rates on the U.S. Mid-Atlantic Shelf increased 15- to 50-fold relative to the late Paleocene[14]. Intense erosion of terrestrial soils and bedrock delivered not only large amounts of siliciclastic sediment and mercury (as shown above) but also terrestrial carbon to the coastal ocean, including fossil carbon (kerogen) from ancient sedimentary rocks[14] and soil carbon/autochthonous carbon[44]. Isotopic, molecular and fossil evidence from PETM sediments indicates that fossil carbon may account for approximately 28–63% of total organic carbon[45]. This is consistent with our conclusion, derived from the Hg isotope mixing model, that more than half of the Hg

was derived from terrestrial soil or fossil carbon erosion. The estimated additional CO_2 release from fossil carbon oxidation during transport spans two orders of magnitude and ranges from 10^2 to 10^4 Pg C[14]. The poorly constrained sediment accumulation rates, shelf area, and oxidation efficiency during transport contribute significantly to the uncertainty in these estimates.

We can here attempt to quantify the magnitude of mobilized terrestrial carbon during the PETM and to quantify the contribution of soil carbon, using a mercury-isotope binary mixing model (Δ^{199}Hg) to calculate the terrestrial mercury fraction (f_{terr}). Combining mercury concentration, linear sedimentation rate (LSR), dry bulk density and depositional duration, we obtained the terrestrial mercury flux. We assume negligible Hg loss occurs during erosion and transport[46], in contrast to organic carbon (15–85% loss), we then used the global mean soil Hg:TOC ratio to estimate the amount of organic carbon associated with the Hg input. Subsequently, this is combined with organic-matter oxidation efficiencies of ref. 57 to back-calculate the potential CO_2 input, which was finally upscaled to the global shelf area (A) to compare our total carbon release to that of Lyons et al.[14]. Three scenarios were constructed: Passive margin (lower limit, LSR = 8.2 cm/kyr, median f_{terr} = 45–56%, L = 50%, A = 2.35×10¹³ m²); Average scenario (LSR = 20.5 cm/kyr, average f_{terr} = 55–60%, L = 60%, A = 3.52×10¹³ m²); Active margin (upper limit, LSR = 32.8 cm/kyr, median f_{terr} = 64–70%, L = 70%, A = 4.69×10¹³ m²). Detailed calculations are provided in the Supplemental Note 4.

Monte Carlo simulations (endmember variability ± 0.10‰) of the mercury isotope mixing model for three sites on the U.S. Mid-Atlantic Shelf (WL, SDB, CD) yielded low median f_{terr} values during the pre-PETM: WL = 45% (36–55%), SDB = 25% (18–34%), CD = 28% (20–37%), indicating limited terrestrial carbon input. During the PETM, f_{terr} increased substantially: WL = 59% (51–69%), SDB = 55% (46–64%), CD = 60% (51–69%). This shows that more than half of the mercury delivered to the shelf during the PETM came from terrestrial sources, and that the associated terrestrial carbon was also transported to the ocean in large quantities. Under the average scenario, the unit-area oxidized carbon ($C_{oxidized}$) was WL = 3.62×10⁴ g/m², SDB = 3.77×10⁴ g/m², CD = 4.79×10⁴ g/m² — about two orders of magnitude higher than pre-PETM background values (~ 9.0×10² g/m²). The highest $C_{oxidized}$ value at CD is consistent with its higher mercury concentration (23.2 ng/g) and f_{terr} (60%), possibly reflecting proximity to a paleo-estuary or preferential deposition of fine-grained, carbon-rich sediment. These site-to-site differences reveal significant spatial heterogeneity in terrestrial carbon mobilization and oxidation even within the U.S. Mid-Atlantic Shelf.

Global total oxidized carbon under the passive margin scenario (lower limit) is 340–395 Pg C; under the average scenario, 1,270–1,690 Pg C; under the active margin scenario (upper limit), 4,420–4,750 Pg C. Compared to pre-PETM, the average scenario yields a net increase of ~ 1,400 Pg C, and the active margin scenario a net increase of ~ 4,520 Pg C (Fig. 5). While these upscaled estimates carry significant uncertainties, the range of oxidized carbon as derived from Hg-MIF signals on the NJ shelf is quantitatively consistent with previous organic biomarker-based evidence for organic carbon oxidation.

Our data from the Atlantic Coastal Plain, showing elevated Hg signals and significant negative isotope shifts, provide evidence for increased terrestrial Hg input during the PETM. The proposed scenario is as follows (Fig. 6): Before the CIE, with relatively low atmospheric carbon dioxide concentrations and precipitation, terrestrial Hg/carbon flux was relatively minimal. The average terrestrial contribution to the total mercury flux is ~ 33%. The estimated carbon oxidation loss per unit area is extremely low (< 0.1 g/m^2). The Mid-Atlantic Shelf primarily received Hg from atmospheric Hg(II) wet deposition, while inputs from air-sea exchange (Hg(0)) and terrestrial riverine sources were relatively minor, resulting in positively skewed Δ^{199}Hg values. During the PETM, the global warming[3], an intensified hydrological cycle[47] and terrestrial ecosystem disturbance led to enhanced erosion and terrestrial Hg input. The average terrestrial contribution to the total mercury flux is ~ 58%. This surpassed the increased atmospheric Hg(II) wet deposition to become the dominant flux of Hg into the ocean, resulting in the anomalous sedimentary Hg enrichments and significant negative Hg isotope excursion. Enhanced terrestrial carbon sources (fossil carbon and soil carbon) underwent intensified oxidation during transport to the shelf, resulting in an increase of the estimated carbon oxidation loss per unit area by dozens of times (> 3.62 g/m^2). Our estimates arrive at ~ 1400 Pg C release under an average scenario. The Hg enrichment in sediments during the PETM on the New Jersey shelf was predominantly driven by terrestrial inputs, suggesting that the enrichment phenomenon may be associated with environmental feedback mechanisms as a result of climate change.

The average-scenario (1,400 Pg C) supports the view that the terrestrial erosion-oxidation feedback may have been an important driver of PETM hyperthermal duration. However, our active-margin total is less than half of the upper limit (10^4 Pg C) reported by Lyons et al.[14], but this difference is mostly due to different density assumptions (2.65 g/cm^3 grain density[14] *vs* 1.7 g/cm^3 dry bulk density in this study see Supplemental Note 4). Given the substantial spatial heterogeneity in terrestrial erosion and carbon oxidation[13] (e.g., up to 34% difference in net carbon release among our three sites), our assumed global shelf area ($2.35–4.69\times10^{13}$ m^2) and sedimentation rates (based primarily on the U.S. Mid-Atlantic shelf) should be considered rough estimates of a global average. Moreover, fluvial fluxes, hydrological intensity, sediment redox conditions and carbon oxidation losses vary greatly across different shelves[14, 48], highlighting the significant challenges in further constraining terrestrial carbon oxidation.

Despite the large uncertainties on the estimates, the Hg data provide independent support for previous estimates and confirm that the upper end of carbon release from terrestrial carbon oxidation estimates might suffice to sustain anomalous conditions while the average (1,400 Pg C) would also appreciably contribute to the long duration of the PETM CIE[45]. Using the cumulative PETM carbon emission inferred from boron-isotope-based paleo-pH reconstructions (~ 10,200 Pg C[7]) as a reference, our maximum active-margin terrestrial carbon oxidation (~ 4,750 Pg C) accounts for less than half of that total. This supports the notion that the PETM was the result of multiple sizeable carbon sources and sinks acting at different rates and times during the event. Besides mobilization of terrestrial carbon, there is evidence for a number of carbon sources of similar order of magnitude; NAIP magmatic carbon and thermogenic volatiles[49], methane hydrate dissociation[50, 51] and vegetation loss[12, 52]. Each of these likely appreciably

contributed to the shaping the PETM carbon cycle perturbation. Both our mercury isotope evidence and the biomarker thermal maturity data from Lyons et al.[14] independently and robustly document large-scale mobilization, transport and oxidation of terrestrial carbon, yielding several hundred to thousands of Pg C spread over the duration of the PETM. Mercury concentration and Hg isotope data, integrated with other lines of evidence and under specific conditions, can provide key independent support for organic and other metal proxies that mobilization of terrestrial carbon from soils and ancient sedimentary rocks constitutes an important positive climate-carbon cycle feedback process.

Declarations

Acknowledgments

The authors thank James Browning and Jean Self-Trail for help during sampling.

Funding Statement

CLM would like to thank the College of Charleston's Summer Undergraduate Research Fund for support. TRT would like to thank the College of Charleston's Faculty Research and Development grant scheme for support as well as the Department of Geology and Environmental Geosciences for startup funds.

Author Contributions

TRT and CLM collected the samples. YJG and CNZ conceived of and supervised the research. YJG and CNZ wrote the original draft. YJG and RYS conducted chemical and isotope analyses. YJG, TRT, CNZ, JF, TJA contributed to the carbon analysis, revised the manuscript, and all authors contributed to the manuscript until its final version.

Competing interests: The authors declare that they have no competing interests.

Data and materials availability: All data needed to evaluate the conclusions in the paper are present in the paper and/or the Supplemental Materials.

References

1. McInerney FA, Wing SL. The Paleocene-Eocene Thermal Maximum: A Perturbation of Carbon Cycle, Climate, and Biosphere with Implications for the Future. In: *Annual Review of Earth and Planetary Sciences, Vol 39* (eds Jeanloz R, Freeman KH) (2011).
2. Frieling J*, et al.* Widespread Warming Before and Elevated Barium Burial During the Paleocene-Eocene Thermal Maximum: Evidence for Methane Hydrate Release? *Paleoceanography and Paleoclimatology*, (2019).
3. Frieling J*, et al.* Extreme warmth and heat-stressed plankton in the tropics during the Paleocene-Eocene Thermal Maximum. *Science Advances*, (2017).

4. Barefoot EA*, et al.* Evidence for enhanced fluvial channel mobility and fine sediment export due to precipitation seasonality during the Paleocene-Eocene thermal maximum. *Geology* **50**, 116-120 (2022).
5. Walters GL, Kemp SJ, Hemingway JD, Johnston DT, Hodell DA. Clay hydroxyl isotopes show an enhanced hydrologic cycle during the Paleocene-Eocene Thermal Maximum. *Nature Communications* **13**, (2022).
6. Pogge von Strandmann PAE*, et al.* Lithium isotope evidence for enhanced weathering and erosion during the Paleocene-Eocene Thermal Maximum. *Science Advances*, (2021).
7. Gutjahr M*, et al.* Very large release of mostly volcanic carbon during the Palaeocene-Eocene Thermal Maximum. *Nature* **548**, 573-577 (2017).
8. Westerhold T*, et al.* An astronomically dated record of Earth's climate and its predictability over the last 66 million years. *Science*, (2020).
9. Kender S*, et al.* Paleocene/Eocene carbon feedbacks triggered by volcanic activity. *Nature Communications* **12**, (2021).
10. Frieling J, Svensen HH, Planke S, Cramwinckel MJ, Selnes H, Sluijs A. Thermogenic methane release as a cause for the long duration of the PETM. *Proceedings of the National Academy of Sciences of the United States of America* **113**, 12059-12064 (2016).
11. DeConto RM*, et al.* Past extreme warming events linked to massive carbon release from thawing permafrost. *Nature* **484**, 87-91 (2012).
12. Nelissen M*, et al.* Widespread terrestrial ecosystem disruption at the onset of the Paleocene–Eocene Thermal Maximum. *Proceedings of the National Academy of Sciences of the United States of America*, (2026).
13. Hollingsworth EH*, et al.* Spatial and Temporal Patterns in Petrogenic Organic Carbon Mobilization During the Paleocene-Eocene Thermal Maximum. *Paleoceanography and Paleoclimatology*, (2024).
14. Lyons SL*, et al.* Palaeocene–Eocene Thermal Maximum prolonged by fossil carbon oxidation. *Nature Geoscience*, (2018).
15. Them TR*, et al.* Terrestrial sources as the primary delivery mechanism of mercury to the oceans across the Toarcian Oceanic Anoxic Event (Early Jurassic). *Earth and Planetary Science Letters* **507**, 62-72 (2019).
16. Jin S*, et al.* Spatiotemporal distribution of global mercury enrichments through the Paleocene-Eocene Thermal Maximum and links to volcanism. *Earth-Science Reviews*, (2023).
17. Jones MT*, et al.* Mercury anomalies across the Palaeocene-Eocene Thermal Maximum. *Climate of the Past* **15**, 217-236 (2019).
18. Jin SM*, et al.* Mercury isotope evidence for protracted North Atlantic magmatism during the Paleocene-Eocene Thermal Maximum. *Earth and Planetary Science Letters* **602**, (2023).
19. Tremblin M*, et al.* Mercury enrichments of the Pyrenean foreland basins sediments support enhanced volcanism during the Paleocene-Eocene thermal maximum (PETM). *Global and Planetary*

Change, (2022).

20. Jin X*, et al.* Early Jurassic massive release of terrestrial mercury linked to floral crisis. *Earth and Planetary Science Letters*, (2022).
21. Bralower TJ*, et al.* Evidence for Shelf Acidification During the Onset of The Paleocene-Eocene Thermal Maximium. *Paleoceanography and Paleoclimatology* **33**, 1408-1426 (2018).
22. Sluijs A*, et al.* Environmental precursors to rapid light carbon injection at the Palaeocene/Eocene boundary. *Nature* **450**, 1218-U1215 (2007).
23. John CM, Banerjee NR, Longstaffe FJ, Sica C, Law KR, Zachos JC. Clay assemblage and oxygen isotopic constraints on the weathering response to the Paleocene-Eocene thermal maximum, east coast of North America. *Geology*, (2012).
24. Stassen P, Thomas E, Speijer RP. Paleocene–Eocene Thermal Maximum environmental change in the New Jersey Coastal Plain: benthic foraminiferal biotic events. *Marine Micropaleontology*, (2015).
25. Self-Trail JM*, et al.* Shallow marine response to global climate change during the Paleocene-Eocene Thermal Maximum, Salisbury Embayment, USA. *Paleoceanography and Paleoclimatology*, (2017).
26. Doubrawa M, Stassen P, Robinson M, Speijer R. Paleoenvironmental and Paleoecological Dynamics of the U.S. Atlantic Coastal Plain Prior to and During the Paleocene-Eocene Thermal Maximum. *The Journal of Foraminiferal Research* **54**, 143-171 (2024).
27. Kopp RE*, et al.* An Appalachian Amazon? Magnetofossil evidence for the development of a tropical river-like system in the mid-Atlantic United States during the Paleocene-Eocene thermal maximum. *Paleoceanography and Paleoclimatology*, (2009).
28. Rush WD, Kiehl JT, Shields CA, Zachos JC. Increased frequency of extreme precipitation events in the North Atlantic during the PETM: Observations and theory. *Palaeogeography, Palaeoclimatology, Palaeoecology*, (2021).
29. Sharman GR*, et al.* Coastal response to global warming during the Paleocene-Eocene Thermal Maximum. *Palaeogeography, Palaeoclimatology, Palaeoecology*, (2023).
30. Stassen P, Thomas E, Speijer RP. Integrated stratigraphy of the Paleocene-Eocene thermal maximum in the New Jersey Coastal Plain: Toward understanding the effects of global warming in a shelf environment. *Paleoceanography* **27**, (2012).
31. Fendley IM, Frieling J, Mather TA, Ruhl M, Hesselbo SP, Jenkyns HC. Early Jurassic large igneous province carbon emissions constrained by sedimentary mercury. *Nature Geoscience* **17**, 241-248 (2024).
32. Sun R, Jiskra M, Amos HM, Zhang Y, Sunderland EM, Sonke JE. Modelling the mercury stable isotope distribution of Earth surface reservoirs: Implications for global Hg cycling. *Geochimica et Cosmochimica Acta*, (2019).
33. Yin R*, et al.* Mercury Isotopes as Proxies to Identify Sources and Environmental Impacts of Mercury in Sphalerites. *Scientific Reports*, (2016).

34. Zheng W, Zhao YQ, Sun RY, Chen JB. The Mechanism of Mercury Stable Isotope Fractionation: A Review. *Bulletin of Mineralogy□Petrology and Geochemistry* **40**, 21 (2021).
35. Fung MK, Schaller MF, Hoff CM, Katz ME, Wright JD. Widespread and intense wildfires at the Paleocene-Eocene boundary. *Geochemical Perspectives Letters*, (2019).
36. Moore EA, Kurtz AC. Black carbon in Paleocene–Eocene boundary sediments: A test of biomass combustion as the PETM trigger. *Palaeogeography, Palaeoclimatology, Palaeoecology*, (2008).
37. Willard D*, et al.* Terrestrial Ecosystem Response to Changing Temperature and Seasonality in the Paleocene-Eocene Thermal Maximum: Shallow Marine Records From the Salisbury Embayment, USA. *Paleoceanography and Paleoclimatology* **41**, (2026).
38. Mastalerz M, Drobniak A, Filippelli G. Mercury content and petrographic composition in Pennsylvanian coal beds of Indiana, USA. *International Journal of Coal Geology*, (2006).
39. Gao X*, et al.* Tracing the source and transport of Hg during pedogenesis in strongly weathered tropical soil using Hg isotopes. *Geochimica et Cosmochimica Acta*, (2023).
40. Tian Z*, et al.* Mercury abundance and isotopic composition in granitic rocks: Implications for Hg cycling in the upper continental crust. *Geochimica et Cosmochimica Acta*, (2023).
41. Soerensen AL*, et al.* An improved global model for air-sea exchange of mercury: high concentrations over the North Atlantic. *Environmental Science & Technology*, (2010).
42. Shen J, Yin RS, Algeo TJ, Svensen HH, Schoepfer SD. Mercury evidence for combustion of organic-rich sediments during the end-Triassic crisis. *Nature Communications* **13**, (2022).
43. Liu MD, Zhang QR, Maavara T, Liu SD, Wang XJ, Raymond PA. Rivers as the largest source of mercury to coastal oceans worldwide. *Nature Geoscience* **14**, 672-677 (2021).
44. Denis EH*, et al.* Decreased soil carbon in a warming world: Degraded pyrogenic carbon during the Paleocene-Eocene Thermal Maximum, Bighorn Basin, Wyoming. *Earth and Planetary Science Letters*, (2021).
45. Baczynski AA*, et al.* Distortion of carbon isotope excursion in bulk soil organic matter during the Paleocene-Eocene thermal maximum. *GSA Bulletin*, (2016).
46. Lawson NM, Mason RP, Laporte J-M. The fate and transport of mercury, methylmercury, and other trace metals in Chesapeake Bay tributaries. *Water Research*, (2001).
47. McInerney FA, Wing SL. The Paleocene-Eocene Thermal Maximum: A Perturbation of Carbon Cycle, Climate, and Biosphere with Implications for the Future. *Annual Review of Earth and Planetary Sciences*, (2011).
48. Rabouille C*, et al.* Comparison of hypoxia among four river-dominated ocean margins: The Changjiang (Yangtze), Mississippi, Pearl, and Rhône rivers. *Continental Shelf Research*, (2008).
49. Svensen H*, et al.* Release of methane from a volcanic basin as a mechanism for initial Eocene global warming. *Nature*, (2004).
50. Dickens G, O'Niel J, Rea D, Owen R. Dissociation of oceanic methane hydrate as a cause of the carbon isotope excursion at the end of the Paleocene. *Paleoceanography* **10**, 965-971 (1995).

51. Thomas DJ, Zachos JC, Bralower TJ, Thomas E, Bohaty S. Warming the fuel for the fire: Evidence for the thermal dissociation of methane hydrate during the Paleocene-Eocene thermal maximum. *Geology*, (2002).
52. Rogger J, Korasidis VA, Bowen GJ, Shields CA, Gerya TV, Pellissier L. Loss of vegetation functions during the Paleocene–Eocene Thermal Maximum. *Nature Communications*, (2025).
53. Gleason JD, *et al.* Sources and cycling of mercury in the paleo Arctic Ocean from Hg stable isotope variations in Eocene and Quaternary sediments. *Geochimica et Cosmochimica Acta*, (2017).

Figures

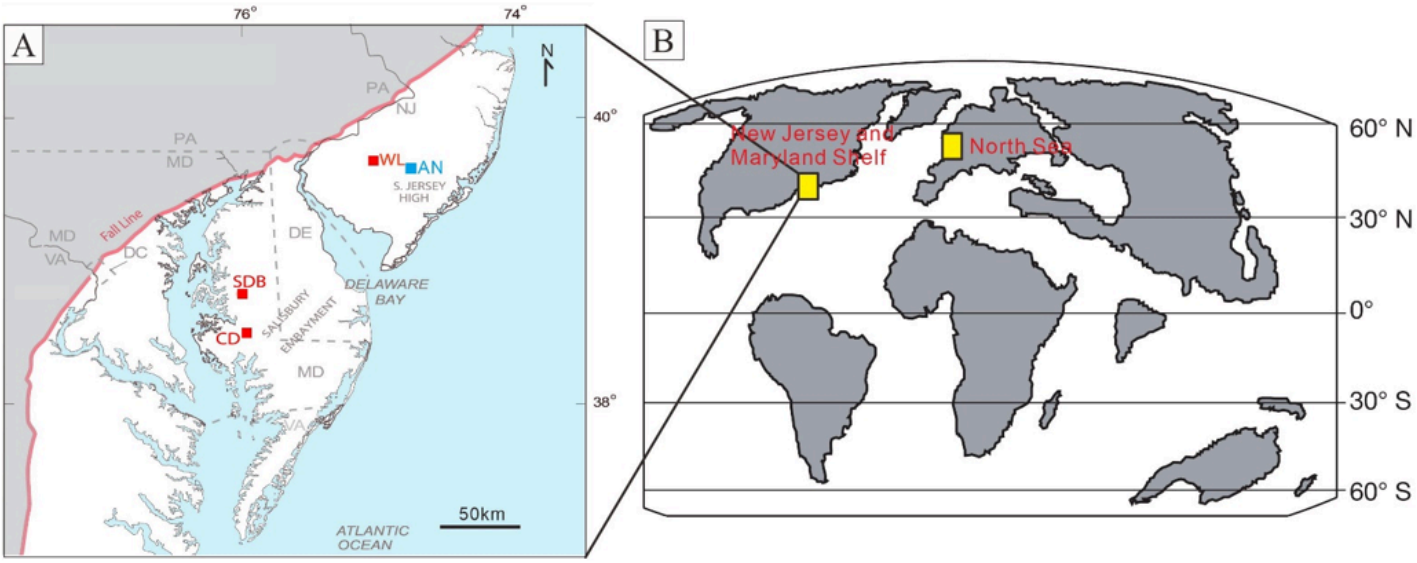


Figure 1

The U.S. Mid-Atlantic Shelf (New Jersey and Maryland) with the core locations (A) and paleogeography (B) during the PETM (~55.9 Ma) (modified after[16, 21, 22]). The red boxes in A represent the three study sites. The blue box indicates the Ancora (AN) site, adjacent to WL, which was used in this paper for the Hg-Al correlation analysis. The yellow boxes in B mark the only two current global locations with systematic Hg isotope studies from the PETM period: the New Jersey and Maryland Shelf from this study and the North Sea 23/16b-9 borehole[18]. Only one Hg isotope data point has been reported from the Arctic ACEX site[53].

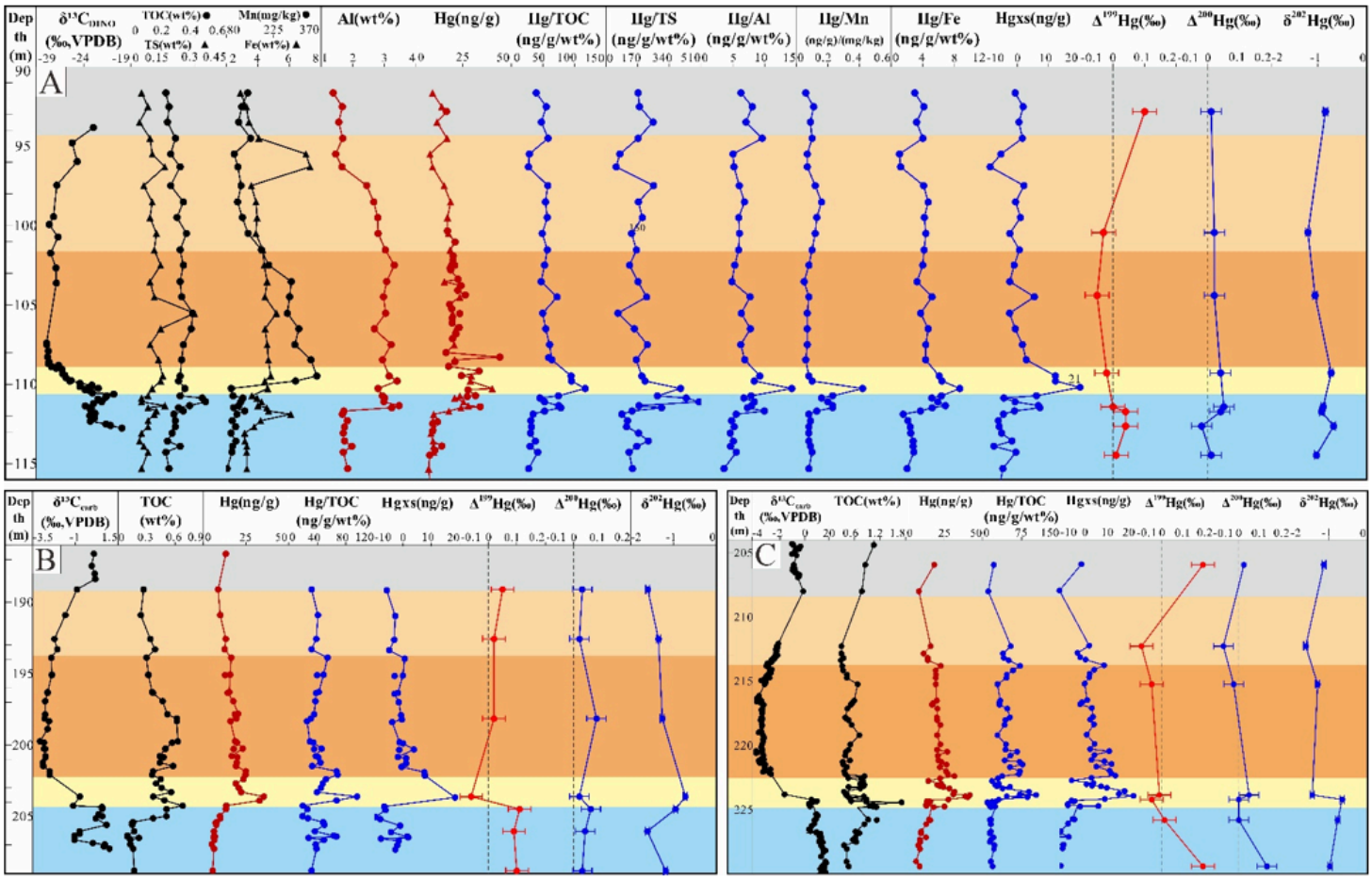


Figure 2

The geochemical records from the PETM at the WL(C), SDB (D), and CD (E) sites. For WL, carbon isotope data (DINO for dinocysts, carb for carbonate), TOC, and major and trace element data are from[14, 16, 22]. Hg concentration data for WL are from[16] (red triangles) and this study (red circles). Carbon Isotope and TOC data for SDB and CD are from[14, 16, 22]. Hg isotope data and Hg concentration data for SDB and CD are from this study. Error bars indicate 2 standard deviations (2sd) of Δ^{199}Hg, Δ^{200}Hg and δ^{202}Hg are 0.08‰, 0.07‰ and 0.09‰, respectively. The dashed lines on the isotope data represent the zero value.

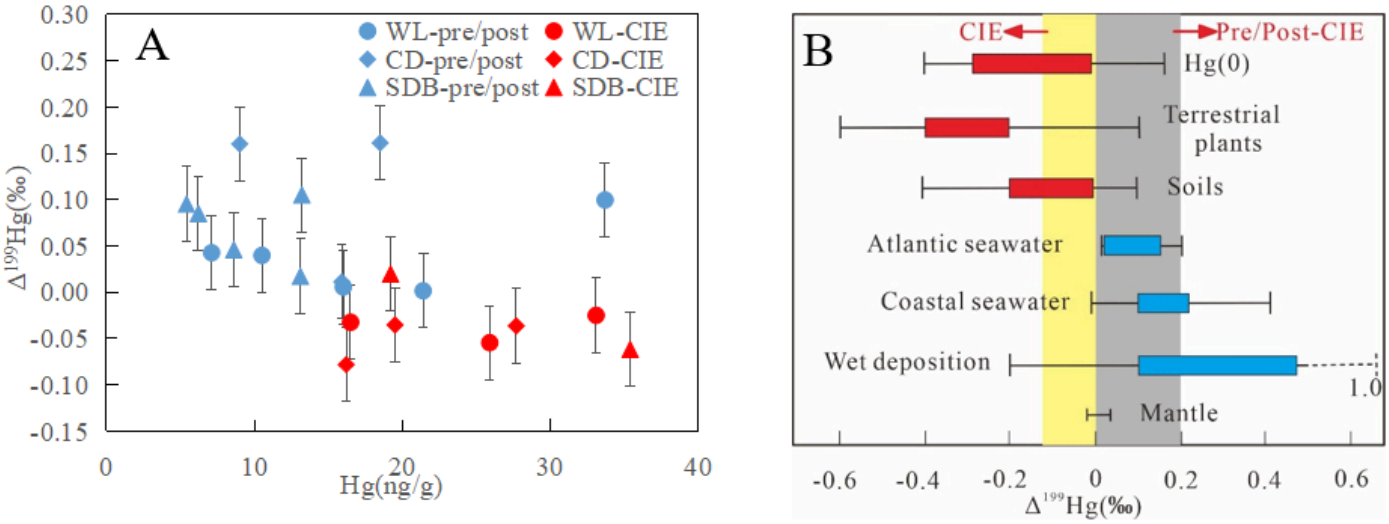


Figure 3

Hg and host-phase element geochemical data. (**A**) Significant differences in sediment Δ^{199}Hg for the three study sites; pre denotes pre-CIE, and post denotes post-CIE; (**B**) Comparative ranges of Δ^{199}Hg for Hg(0), terrestrial plants, soils, coastal seawater, wet deposition, and mantle, adapted from[32, 33]). Note the difference in Δ^{199}Hg between the yellow vertical box (CIE) and the green vertical box (pre/post-CIE). Error bars indicate confidence intervals; the red or blue horizontal boxes represent the interquartile range.

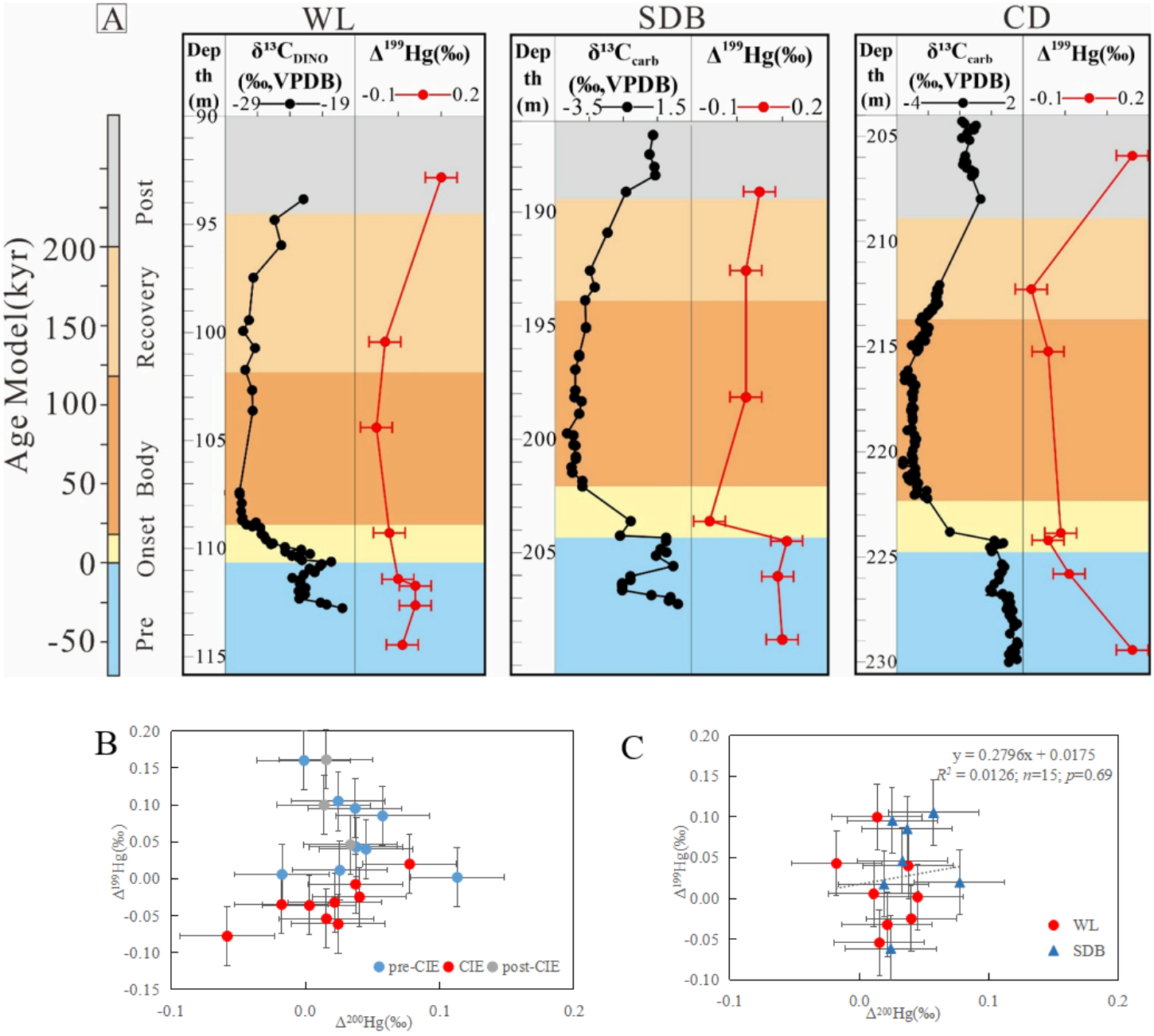


Figure 4

Chronological comparison of the sequence of odd-Hg isotope negative excursions (A), based on the age model from [16] and even Hg isotope correlations (B-C). (**A**) The stratigraphic column from base to top is color-coded as follows: blue (pre-CIE), brown (CIE) and gray (post-CIE), representing different phases of the PETM carbon isotope excursion on an idealized timeline. (**B**) Distribution of Δ^{199}Hg vs. Δ^{200}Hg data in sediments from the three study sites; (**C**) Δ^{199}Hg *versus* Δ^{200}Hg data for the WL and SDB sites.

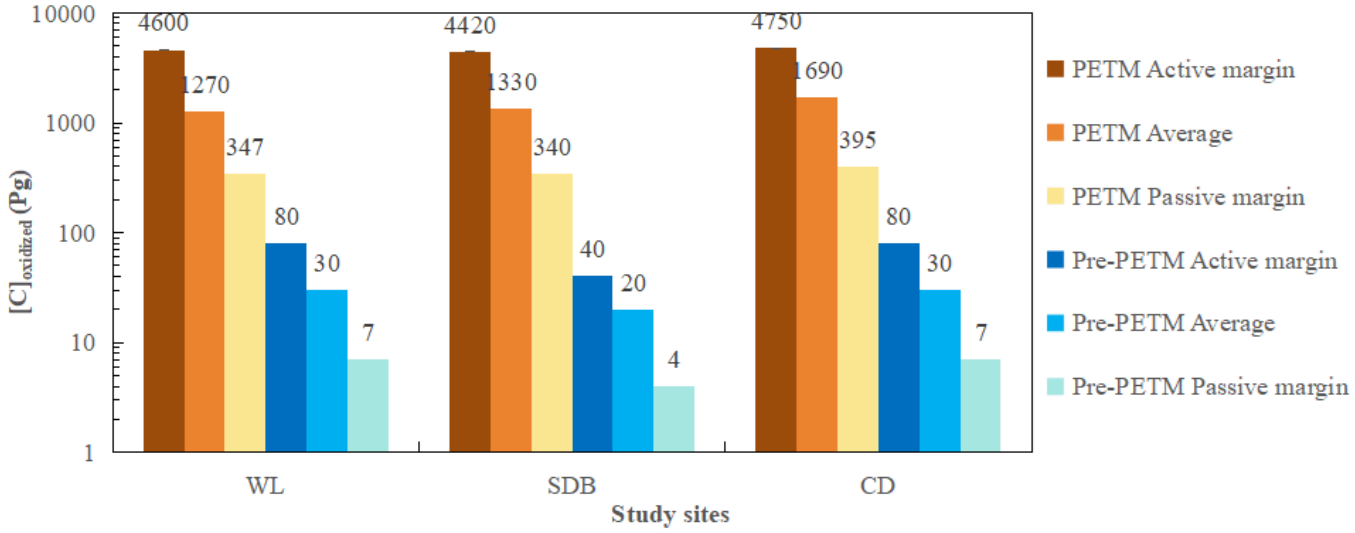


Figure 5

The amounts of carbon released from terrestrial carbon oxidation during the PETM and pre-PETM interyals (100 kyr), calculated separately using the three study sites (WLB, CD, SDB) on the Mid-Atlantic Shelf.

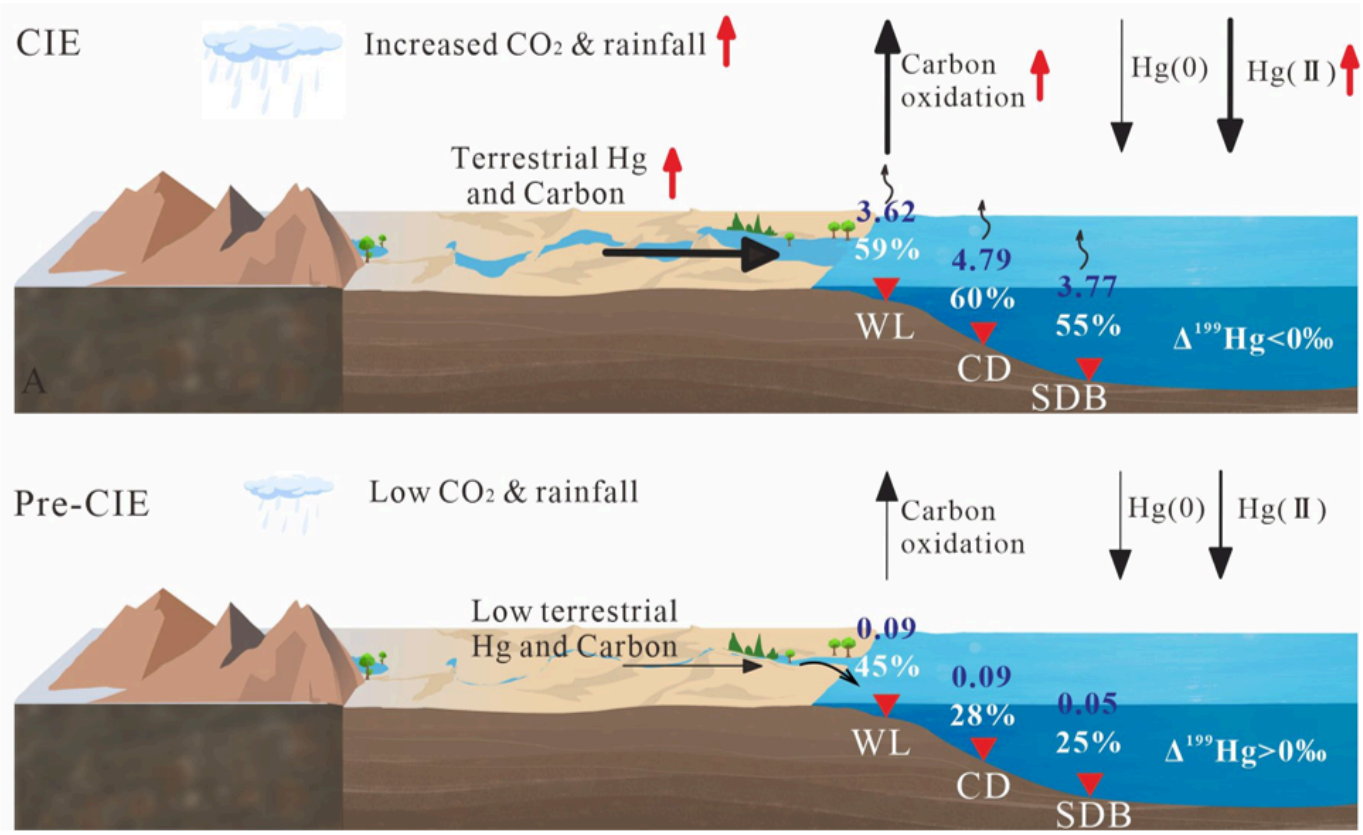


Figure 6

Terrestrial mercury and carbon flux variations across the PETM. The schematic diagram illustrates continental configurations and ocean during this period. Red inverted triangles mark the approximate paleogeographic positions of the three study sites (WLB, CD, SDB) on the Mid-Atlantic Shelf. Black arrows denote mercury or carbon fluxes, with arrow thickness reflecting the magnitude of the flux. Red upward-pointing arrows indicate enhanced processes (e.g., terrestrial runoff, mercury loading, or carbon oxidation release). White numbers (e.g., 45%) represent the proportion of terrestrial terrestrial mercury in total mercury (f_{terr}) and Hg isotopes, and the blue numbers above them indicate the estimated carbon oxidation loss per unit area (g/m^2).

Supplementary Files

This is a list of supplementary files associated with this preprint. Click to download.

- DataS1.xlsx
- DataS2.xlsx
- 2026.4.24PETMSIJF2.docx
- 2026.4.24PETMSIJF2tja.docx